2004 SCEC REPORT

Southern California Tectonic Deformation Modeling

Zheng-Kang Shen and **David D. Jackson**

Department of Earth and Space Sciences, UCLA

We analyze velocity of field southern California presented in the SCEC Crustal Motion Map v3.0 (CMM3) using two approaches. The first approach is a continuation of modeling secular crustal deformation using a linked-fault-segment model. In this approach surface deformation is associated with dislocation along fault segments beneath the locking depth. Fault slip continuity is enforced by imposing finite constraints on slips along adjacent fault segments. Two end members emerge depending on the degree of constraints: strict constraints leads to a block-fault model, and loose constraints yields fault-segment-only model. Thus by optimally adjusting the degree of constraints, we are able to adopt the model to describe deformation not exactly "block-like", yet still limiting the number of free parameters in the model. Major improvement of the model this year is on optimization of fault geometry. Our fault geometry was synthesized from numerous previous geological and geodetic studies. Fault geometry has been improved significantly by the SCEC focus group of Structure Representations through a series updates of the SCEC Community Fault Model (CFM) and Community Block Model (CBM), particularly in the Western Transverse Ranges area. Because many geological faults are presented in the region, we have tested different routes to connect the faults forming block boundaries, and used CMM3 data to invert for the fault slip rates. After tens of trials on different fault combinations we obtained the optimal model determined using F-test on the data postfit residual chi-squares and model resolution. We performed such inversions on data sets both before and after the 1992 Landers earthquake. The results are shown in Table 1.

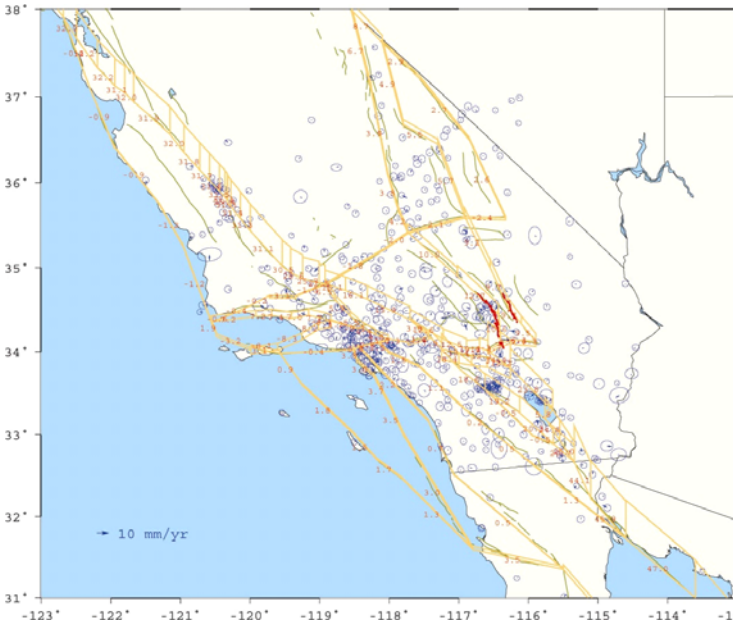

Figure 1. Post-Landers fault modeling result: strike slip component. Orange patches are modeled fault slip rates beneath locking depth, and their heights are proportional to the amplitudes of the slip rates. The number on each patch denotes its slip rate, right lateral positive. Red curves are the Landers and Hector Mine surface rupture traces. Blue arrows are postfit residuals of the velocity data. Error ellipses represent 95% confidence.

We then compared our new model result with the one we obtained last year, and find that major deformation patterns of the two models are pretty much the same. They include: (a) slip rate changed along the SAF after the Landers earthquake, increased along the sections of Coachella Valley from 20 to 24 mm/yr and Carrizo Plain from 27 to 31 mm/yr, and decreased along the Mojave section from 20 to 16 mm/yr; (b) deformation rate across the Mojave Shear Zone changed significantly after the Landers earthquake, fault slip rate along the Blackwater fault increased from 8 to 13 mm/yr; (c) slip rate decreased along the San Jacinto fault by about 3 mm/yr after the quake, etc. We also report that among the fault normal components which are more reliably resolved, significant convergence is detected across the Santa Susana fault at ~9 mm/yr, Cucamonga fault at ~7 mm/yr, Santa Cruz fault at ~7 mm/yr, and San Cayetano fault at ~5 mm/yr, respectively (Table 1).

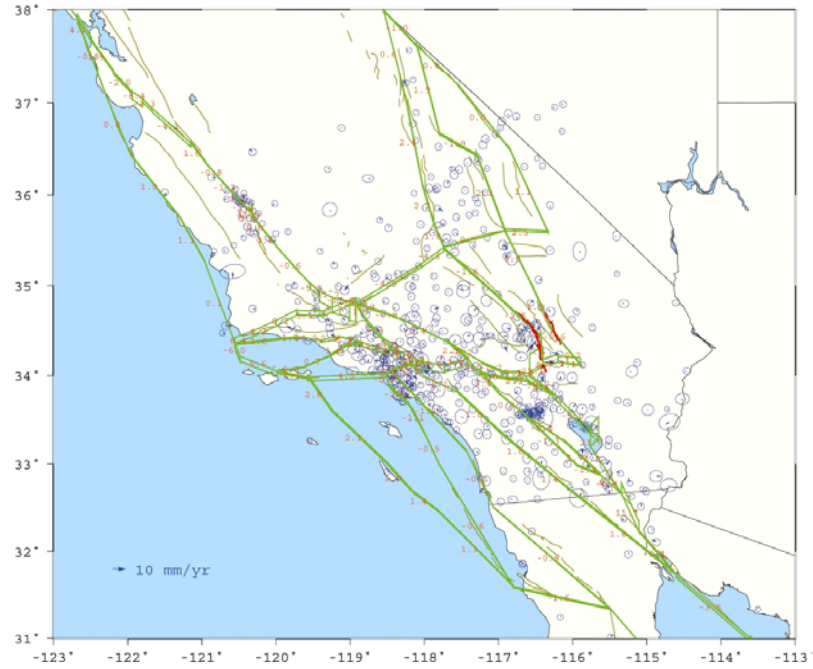

Figure 2. Post-Landers fault modeling result: normal component. Green patches are modeled fault slip rates beneath locking depth, and their heights are proportional to the amplitudes of the slip rates. The number on each patch denotes its slip rate, extension positive. The rest captions are the same as above.

Table 1. Fault slip rates

Fault	Post-Landers				Pre-Landers				Fault	Post-Landers				Pre-Landers			
	Vr	Vn	Rvr	Rvn	Vr	Vn	Rvr	Rvn		Vr	Vn	Rvr	Rvn	Vr	Vn	Rvr	Rvn
SAF-North	32	0	0.17	0.22	42	1	0.07	0.01	Anacapa-Santa-Cruz	0	-5	0.52	0.42	-1	-4	0.34	0.22
SAF-Parkfield	31	0	0.39	0.29	28	-1	0.18	0.03	Pinto-Mtn-West	-4	22	0.04	0.12	-1	15	0.03	0.07
SAF-Carrizo	31	0	0.16	0.16	27	0	0.17	0.10	Pinto-Mtn-East	-6	7	0.10	0.19	-1	7	0.02	0.09
SAF-Tajon	26	-17	0.06	0.08	25	-9	0.03	0.02	Oak-Ridge	-8	0	0.49	0.30	-3	0	0.11	0.05
SAF-Mojave	16	0	0.50	0.51	20	0	0.15	0.07	Cucamonga	-4	-7	0.14	0.18	-1	-8	0.13	0.15
SAF-Cajon	13	-3	0.33	0.39	14	-2	0.03	0.01	Sierra-Madre	4	-7	0.09	0.06	-2	2	0.06	0.02
Banning	-13	0	0.27	0.15	-9	1	0.05	0.01	San-Gabriel	6	-3	0.38	0.26	9	0	0.15	0.08
SAF-Coachella V	24	-5	0.53	0.35	20	-3	0.36	0.24	Raymond	-2	3	0.09	0.05	-2	2	0.06	0.02
Brawley	25	0	0.12	0.25	20	1	0.10	0.14	Santa-Monica-Malibu	0	1	0.18	0.22	-3	2	0.14	0.06
Imperial-Valley	46	0	0.34	0.20	43	0	0.05	0.03	Santa-Susana	6	-9	0.11	0.10	8	-7	0.10	0.07
SAF-South	46	3	0.24	0.04	42	1	0.07	0.01	San-Cayetano	1	-5	0.26	0.17	-2	-4	0.07	0.04

Mexico-South	6	0	0.42	0.18	9	0	0.22	0.04	Arroyo	7	-1	0.52	0.24	0	-2	0.08	0.06
San-Clemente	2	2	0.63	0.35	5	-1	0.10	0.04	Big-Pine	-1	5	0.41	0.42	3	4	0.04	0.05
New-Port-Inglewood	2	-1	0.40	0.36	5	-2	0.22	0.16	San-Gregorio-Hosgri	-1	1	0.58	0.49	4	0	0.10	0.11
Whittier	2	0	0.20	0.16	0	0	0.13	0.06	Garlock-West	-2	-4	0.45	0.54	-5	1	0.30	0.31
Elsinore	1	2	0.97	0.69	0	0	0.26	0.06	Garlock-East	-2	2	0.43	0.63	-5	2	0.05	-0.03
SJF-North	18	-4	0.13	0.07	21	-1	0.18	0.05	Owens-Valley	4	2	0.53	0.62	10	0	0.08	0.02
SJF-Central	19	2	0.34	0.17	22	-2	0.39	0.04	Pisgah	9	0	0.39	0.33	7	-2	0.00	0.01
SJF-South	20	0	0.77	0.15	23	-1	0.09	0.04	Blackwater	13	-2	0.57	0.71	8	0	0.21	0.25
Superstition-Hill	4	-1	0.53	0.13	0	-1	0.11	0.00	Hunter-Mtn-Param V	5	0	0.73	0.61	4	-1	0.02	0.02
Palos-Verdes	3	-3	0.13	0.10	0	-1	0.22	0.12	Death-Valley	3	1	0.65	0.68	5	1	0.06	0.02

Vr: Right slip; Vn: fault normal slip; R_{Vr}: right slip resolution; R_{Vn}: fault normal slip resolution

We have also investigated strain rate field by interpolating CMM3 velocity field, to understand strain distribution, particularly at regions where relatively larger residual field is found after our linked-fault-elment modeling. Interpolation is done through a least-squares procedure for each spot, with velocity data in the neighborhood reweighted according to the distance between a geodetic station and the spot being evaluated (Shen et al., 1996). Again the CMM3 velocity field is divided into two groups of pre- and post-Landers earthquake, which are interpolated separately. Figs. 3 illustrates the maximum shear, principal strain, dilation, and rotation rates for the two sets of strain rate field respectively. Results show the following:

1. Dextral shear strains are accumulated fast, up to 0.35 micro-radian/yr, along the Carrizo Plain section of SAF. It is increased along the Coachella Valley, Brawley, and Imperial Valley sections of the fault after the Landers earthquake, from 0.2-0.3 micro-radian/yr to 0.25-0.4 micro-radian/yr. Dextral shear strain is also increased in the Landers epicentral area after the quake, from ~0.1 to ~0.3 micro-radian/yr.
2. Crustal shortening is found along the Western Transverse Ranges, but locations seem to have changed after the Landers earthquake. Up to ~0.15 micro-strain/yr north-south convergence is detected in a region from the Ventura basin to Santa Barbara Channel and in the San Fernando Valley before the quake, the high strain rate region shifted to the epicentral area of the 1994 Northridge earthquake and its surroundings after. This shift likely reflects postseismic deformation following the Northridge earthquake, since the post-Landers data set used in this study were collected primarily after the Northridge event. North-south convergence is also found in the White Wolf fault area both before (~0.1 micro-strain/yr) and after (~0.15 micro-strain/yr) the Landers event, possibly reflecting long lasting post-seismic deformation after the 1952 Kern County earthquake. North-south convergence is shown in the Los Angeles basin for both time periods. About ~0.15 WNW-ESE extension is detected in the San Bernardino Mountains area north of the SAF and Pinto Mountains fault after the Landers quake, possibly reflecting viscous crustal adjustment responding to the quake there. Comparing these regional strain rates with postfit residual field of our linked-fault-element model, we find that regions showing significant postseismic strain signals coincide well with the areas with poorest fitting to the model. Despite the fact that our linked-fault-element model has actually been adjusted to accommodate the postseismic deformation, it seems not enough to absorb that all. This observation, in return, validates that these deformation

patterns are transient, not compatible with a block motion model.

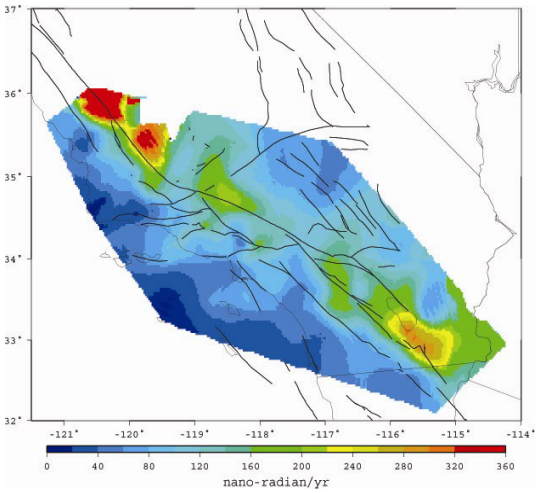

Figure 3a. Pre-Landers maximum shear strain rate.

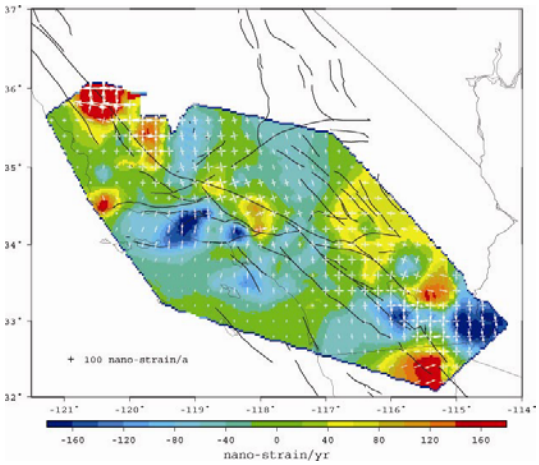

Figure 3b. Pre-Landers principal strain and dilatation rates.

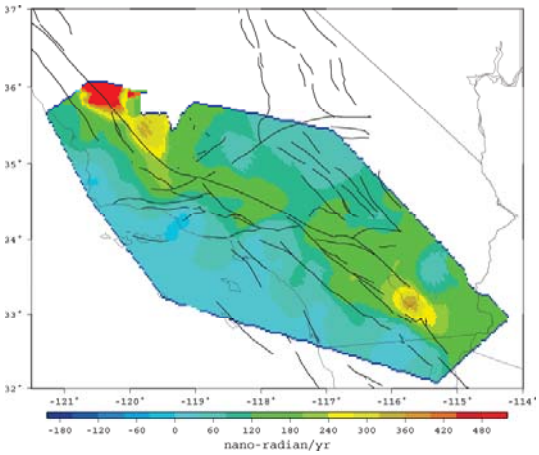

Figure 3c. Pre-Landers rotation rate.

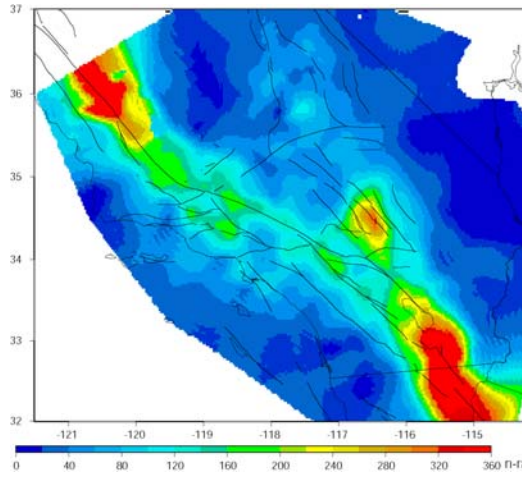

Figure 3d. Post-Landers maximum shear strain rate.

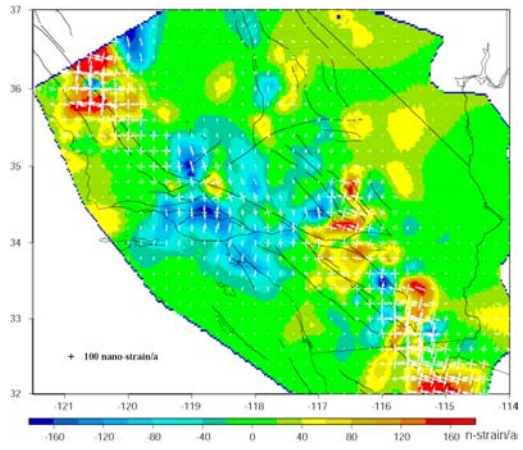

Figure 3e. Post-Landers principal strain and dilatation rates.

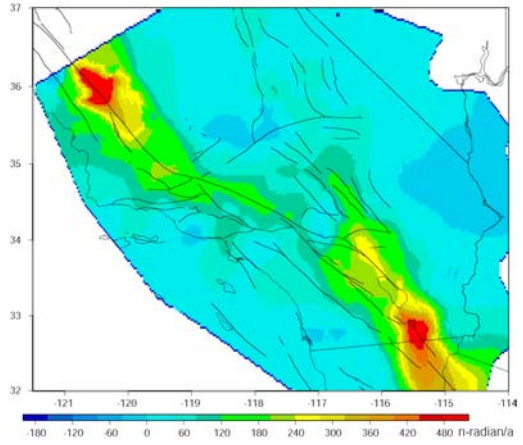

Figure 3f. Post-Landers rotation rate.

3. High clockwise rotation rates are generally associated with faults of fast strike slip such as the SAF and San Jacinto (0.15-0.5 micro-radian/yr), and with post-Landers slip along faults in the Mojave Shear Zone (~0.15 micro-radian/yr). Clockwise rotation seems to have been

reduced since the Landers earthquake in west Mojave Desert area, from ~0.10 to ~0.08 micro-radian/yr. This could be resulted from viscous adjustment of crustal after the Landers quake.